

Available Data (DFSAR): DFSAR is currently acquiring monostatic data from a nominal 100 km circular polar orbit. Since its first imaging season in 2019, DFSAR has been collecting L-band, full polarimetric, high-resolution (25 m/pix) data of the lunar poles from $\pm 75^\circ$ to 90° . To date, $\sim 95\%$ coverage poleward of 85° and $\sim 65\%$ coverage in the latitude range from 80° to 85° has been achieved (Fig. 2, Table 1). Simultaneous dual-frequency (L- and S-band), hybrid-pol (to complement

Mini-RF data), and radiometric data are planned for key targets identified in the polar regions (e.g., PSRs and Artemis zones). Very high resolution DFSAR hybrid-pol acquisitions (4 m/pix ground resolution) are also planned to target landing sites of existing and future missions, similar to those obtained for the rocket booster impact event in March 2022 [7].

Summary: Mini-RF and DFSAR radar data provide fundamental information on the structure and dielectric properties of the lunar surface and buried materials within the penetration depth of the system(s) [e.g., 8-10] and have the advantage of being sensitive to the physical form of water ice [11-13]. Radar data characterize wavelength-scale scatterers (e.g., size-frequency distribution, morphology), provide insights into subsurface structure, and constrains bulk density and composition (i.e., dielectric permittivity), all values relevant for characterizing landing hazards (e.g., Fig. 3 and 4). The continued operation of Mini-RF and the addition of DFSAR in orbit around the Moon provide both complementary and unique capabilities for measuring these properties and for addressing science and engineering objectives of the Artemis and CLPS programs.

References: [1] Raney R. K. et al. (2011) *Proc. IEEE*, 99, 808–823; [2] Putrevu et al. (2016), *ASR*, 57, 627-646; [3] Kirk R. L. et al. (2013) *LPSC XLIII*, Abstract #2920; [4] Hapke et al. (1998), *Icarus*, 133, 89-97; [5] Nelson et al. (2000), *Icarus*, 147, 545-558; [6] Piatek et al. (2004), *Icarus*, 171, 531-545; [7] Chakraborty et al., this LPSC volume; [8] Campbell et al. (2010), *Icarus*, 208, 565-573; [9] Raney et al. (2012), *JGR*, 117, E00H21; [10] Campbell (2012), *JGR*, 117, E06008; [11] Slade et al. (1992), *Science* 258, 635-640; [12] Black et al. (2001), *Icarus* 151, 167-180; [13] Rivera-Valentín, E. G. et al. (2022) *PSJ* 3, 62.

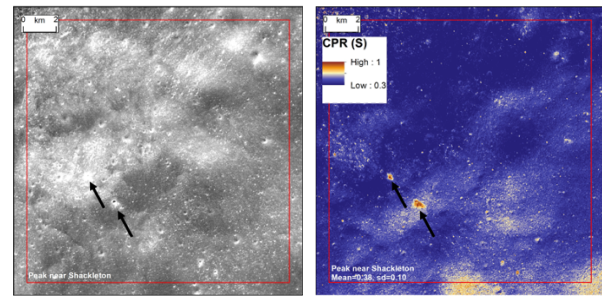


Fig. 3. Mini-RF S-band zoom S_1 (left) and CPR (right) coverage of the landing zone Peak Near Shackleton. CPR data indicates overall low cm-scale surface roughness for the landing zone, with the exception of several prominent fresh craters.

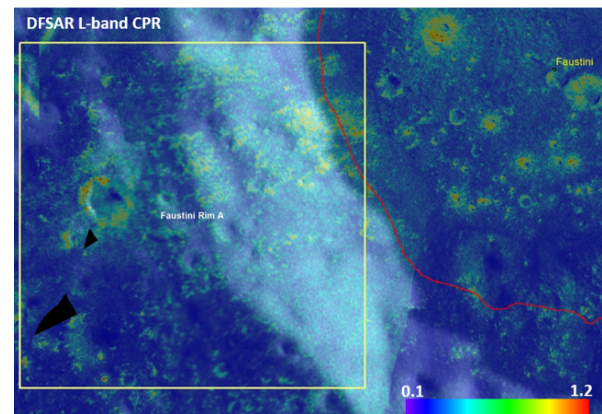


Fig. 4. DFSAR L-band CPR overlain on LROC WAC global mosaic. Artemis landing zone indicated in yellow and boundary of Faustini floor PSR in red. Crater ejecta and mass wasting features are clearly observed.

Table 1. Mini-RF and DFSAR coverage of Artemis landing zones

Radar Architecture		Monostatic				Bistatic	
Wavelength		24 cm*	12.6 cm		4.2 cm	12.6 cm	4.2 cm
Spatial Resolution		25 m	30 m	150 m	30 m	150 m	100 m
Artemis Zones	Amundsen Rim	◇	◆	◇		◆	
	Connecting Ridge	◇	◇			◆	◆
	Connecting Ridge Extension	◇	◇			◆	◆
	de Gerlache Rim	◇	◇			◆	◆
	de Gerlache Rim 2	◆	◆			◆	◆
	de Gerlache-Kocher Massif	◇	◆	◆	◆		
	Faustini Rim A	◆	◆	◆		◇	◇
	Haworth	◇	◆		◇	◆	◆
	Leibnitz Beta Plateau	◇	◆			◆	◆
	Malapert Massif	◆	◆			◆	◆
	Nobile Rim 1	◇	◆			◆	◇
	Nobile Rim 2	◇	◆		◇	◆	
	Peak Near Shackleton	◇	◆	◆		◇	◇

*Opposite look direction coverage is available for DFSAR (24 cm) data but not shown in Fig. 2

◆ Denotes complete coverage of zone

◇ Denotes partial coverage of zone